Energy Technology
Generation, Conversion, Storage, Distribution
www.entechnol.de

Reactive Metals as Energy Storage and Carrier Media: Use of Aluminum for Power Generation in Fuel Cell-Based Power Plants

Linda Barelli, Manuel Baumann, Gianni Bidini, Panfilo A. Ottaviano, Rebekka V. Schneider, Stefano Passerini, and Lorenzo Trombetti*

In recent years, the energy production sector has experienced a growing interest in new energy vectors enabling energy storage and, at the same time, intersectoral energy applications among users. Hydrogen is one of the most promising energy storage and carrier media featuring a very high gravimetric energy density, but a rather low volumetric energy density. To this regard, this study focuses on the use of aluminum as energy storage and carrier medium, offering high volumetric energy density (23.5 kWh L^{-1}), ease to transport and stock (e.g., as ingots), and is neither toxic nor dangerous when stored. In addition, mature production and recycling technologies exist for aluminum. Herein, the performance of power systems driven by aluminum powder in terms of electrical efficiency ($\eta_{(l)}$) and round-trip efficiency (RTE) is analyzed. Along with the additional advantages relating to high volumetric energy density, and safety and management aspects, the aluminum-based technology appears to outperform the power-to-power systems based on hydrogen and liquid fuels.

1. Introduction

The energy production from renewable energy sources (RES) is expected to reach a 31% share in the world-wide energy generation by 2050.[1] However, its exploitation requires relevant system flexibility to bridge the RES geographical and temporal variations. The latter is typically characterized by three different time scales from short-term (seconds up to minutes), mid-term (hours to days), to long-term (weeks to a year or more) fluctuations. This flexibility can only be achieved by a combination of the 1) overall system architecture change, i.e., the increase in both the distributed generation and electrification (grid extension and interconnection); 2) integration of energy storage devices with renewable generation and local users as enabled by smart grids; and 3) the realization of sector coupling in multienergy systems integrating multiple energy vectors and sectors. The achievement of the last objective would enable higher RES amounts in the energy system by providing flexibility, especially on mid- to long-term timeframes, at lower cost and environmental impacts than electricity-only solutions.[2] Therefore, the challenges in the energy production sector include new energy storage and carrier media (ESCM) enabling energy storage and intersectoral applications at the users' side, able to compete with the traditional carriers such as coal, oil, and natural gas.

Since a few decades, green hydrogen is being considered the most promising ESCM candidate to enable the storage of renewable energy on the long-time scale (e.g., seasonal storage), despite only 4% of its current production is based on electrolysis (i.e., possibly from RES).[3] Hydrogen is characterized by a very high gravimetric energy density and, depending on the production path, CO_2-free production,[4] but its volumetric energy density is a critical issue.[5] In contrast, hydrogen can be easily exploited in power-to-power (P2P) systems[6] by several means (fuel cells [FCs], gas turbines [GTs], and so on), but it can also be used in power-to-X (P2X) frameworks such as mobility applications (in form of pure H_2[7,8] or hydromethane[9]) and industrial processes (steel making, oil refining, and ammonia production).

Regarding storage, however, hydrogen liquefaction and compression are still far from achieving volumetric energy

Prof. L. Barelli, Dr. G. Bidini, Dr. P. A. Ottaviano, Dr. L. Trombetti
Department of Engineering
University of Perugia
Via G. Duranti 93, I-06125 Perugia, Italy

Dr. M. Baumann
Institute for Technology Assessment and Systems Analysis
Karlsruhe Institute of Technology (KIT)
Karlstraße 11, D-76131 Karlsruhe, Germany

Dr. M. Baumann, Dr. R. V. Schneider, Prof. S. Passerini
Karlsruhe Institute of Technology (KIT)
P.O. Box 3640, D-76021 Karlsruhe, Germany
E-mail: stefano.passerini@kit.edu

Dr. R. V. Schneider, Prof. S. Passerini
Helmholtz Institute Ulm (HIU)
Helmholtzstrasse 11, D-89081 Ulm, Germany

The ORCID identification number(s) for the author(s) of this article can be found under https://doi.org/10.1002/ente.202000233.

Correction added on 19 August 2020, after first online publication: Projekt Deal funding statement has been added.

DOI: 10.1002/ente.202000233

densities and cost performance comparable with fossil fuels, introducing, at the same time, substantial safety problems (see, e.g., Norwegian hydrogen explosion in June 2019[3] due to an incorrectly mounted plug in a high-pressure hydrogen tank[10]).

Liquifying hydrogen (i.e., cooling it to −253 °C) requires one third of its energy content[11] limiting the overall energy performance[12] to only 2.35 kWh L^{-1}.[13] Hydrogen compression up to 700 bars, corresponding to an energy storage of 1.4 kWh L^{-1} under ambient conditions, is more energy efficient. In fact, using multistage compressors with intercoolers, it implies a lower energy loss (only about 12%) calculated as higher heating value.[14] For completeness, the use of metal hydrides for H_2 storage, especially the low temperature ones,[15] allows storing around 3.5 wt% H_2 corresponding to 1.6 and 4.5 kWh L^{-1}.[16] Among other energy carriers, liquid organic hydrogen carriers are characterized by a 4–7 wt.% hydrogen content.[17] The main drawback of these materials is still the endothermic nature of the dehydrogenation procedure. Methanol is also a promising organic carrier storing 12.5 wt% H_2,[18] exhibiting an energy density of around 4.3 kWh L^{-1} in the liquid phase.[19] The technology for methanol production is well established in the industrial context, but the H_2 reverse synthesis requires an improvement of catalyst materials.[20]

In recent years, a growing interest in inorganic ESCMs has occurred.[21] Ammonia is a carbon neutral fuel and could play an important role as energy carrier in the future, but only if produced from RES. Ammonia is able to store about 17.8 wt% H_2, corresponding to 3.5 kWh L^{-1} at 0.8 MPa and 288 K (5.2 kWh kg^{-1}), but its utilization needs to be improved. In fact, the combustion of ammonia produces large amounts of NO_x,[22] whereas its direct utilization in FCs still needs to overcome the problems related to ammonia emissions and nitrate production at the anode. Anodic endothermic decomposition of ammonia results in alteration of the anode morphology[23] and a significant increase in the Ohmic resistance with cell performance degradation.[24,25]

Aluminum appears to be a rather interesting ESCM, promising better performance and higher safety than hydrogen[5,26] for large scale, global multisectoral energy storage. P2X applications would be favored by the high volumetric energy density of aluminum enabling rather easy and low-cost mid- and long-term storage. This study addresses the development of suitable plants for the re-electrification of aluminum used as energy carrier to provide additional flexibility to the energy sector. Both solid (powder) and molten aluminum are examined for applications in the stationary power generation sector, including the integration of aluminum-based energy storage within aluminum refinement plants.

Two innovative aspects are proposed in this work. The first is the simultaneous exploitation of produced heat and hydrogen, by implementing both low and high temperature FCs, i.e., polymer electrolyte membrane (PEM) and solid oxide FC (SOFC) technologies, respectively. Second, the integration of the metal-to-power system scaled-up to the MW order with an aluminum refinement process allowing liquid aluminum feeding, yielding a further improvement of energy performance. This latter aspect is particularly relevant because the short-term re-electrification of aluminum enables to balance fluctuations of both the RESs and the energy market prices, enhancing the flexibility of the overall energy system.

2. State-of-the-Art of Aluminum as Energy Carrier

Aluminum is produced starting from bauxite, which is one of the most widespread minerals in the Earth's crust. Its chemical combustion via water reaction (Equation (1)) has been extensively studied in the literature[27,28] both in industrial[29] and power generation processes.[30] In particular, 1 kg of Al releases 15.1 MJ of heat, 0.11 kg of H_2, and 1.9 kg of alumina (Al_2O_3) that can be recycled in the aluminum production or sold as pure alumina.

$$2Al_{(s)} + 3H_2O_{(g)} \rightarrow Al_2O_{3(s)} + 3H_{2(g)} - 815.4\frac{kJ}{mol}(298\,K, 1\,atm) \quad (1)$$

The overall volumetric energy density, including the thermal energy from Equation (1) and the oxidation of the resulting hydrogen (e.g., reacted or burned with oxygen), amounts to 23.5 kWh L^{-1} of Al. This value is more than twice and about 10 times those of fossil fuels and liquefied H_2, respectively.[5] However, it should be remarked that the evaluation solely considers the volume of aluminum, i.e., it is suitable only for applications where water is available at the point of use, e.g., marine applications or stationary power generation.

The gravimetric and volumetric energy densities for the complete oxidation of different energy carriers are shown in **Table 1**.

Aluminum–water oxidation (Equation (1)) under standard conditions is hampered due to the passivating oxide surface layer. For this reason, various alternatives to activate aluminum have been investigated, such as chemical methods based on the use of alkaline aqueous solutions, such as NaOH or KOH, have

Table 1. Volumetric energy density (kWh L^{-1}) and gravimetric energy density (kWh kg^{-1}) calculated from the oxidation of different materials.[5,19] For a further comparison, high-performance Li-ion battery cells offer about 0.3 kWh kg^{-1} and 0.8 kWh L^{-1}.

	Grav. energy density [kWh kg^{-1}]	Vol. energy density [kWh L^{-1}]
Zn	1.6	10.7
Fe	2.4	16.7
DOE H_2 target	2.5	2.2
Methanol	4.3	5.5
Biomass	4.8	2.3
Ammonia	5.2	3.5
Coal	7.2	9.1
Mg	7.3	12.6
Al	8.6	23.5
Diesel	11.8	10.0
Gasoline	12.0	8.8
CNG (250 bar)	13.1	2.5
LNG	13.8	5.8
Compressed H_2 (700 bar)	33.4	1.4
Liquefied H_2	33.4	2.3

been proposed.[31–33] Alternatively, metals such as lithium[34,35] and gallium[36,37] can be added in small percentages (maximum of 10 wt%) to the aluminum to activate the reaction, yielding to almost full aluminum conversion even at ambient temperature. However, the aforementioned approaches imply problems associated with corrosive effects and high components wear or cost.

Aluminum activation can also be achieved using coarse powders at high temperatures: nearly 100% H_2 yield can be achieved with particles ranging from 14 to 80 μm at temperatures higher than 200 °C.[28,29,38] In this context, an experimental apparatus has been already implemented to identify the operative conditions appropriate for aluminum powders.[38] The same test reactor has been studied in combination with different power plant schemes,[39,40] allowing the estimation of the electrical efficiency of plants including FCs operating under hydrogen combustion. In particular, complex schemes with heat recovery and binary cycles have shown the highest electrical efficiency (i.e., 40%).[40] This background is used in this work as the starting point for the development of power plants based on the hydrothermal aluminum oxidation reaction.

Regarding the aluminum production, the Hall–Héroult process at industrial scale is considered. The process is operated at 940–980 °C yielding 99.5–99.8% pure aluminum[41] through the electrolysis of alumina (Al_2O_3) dissolved in cryolite (Na_3AlF_6). Carbon anodes, which are consumed during the electrochemical reaction, are immersed into the electrolyte. The produced liquid aluminum deposits at the bottom of the reaction vessel.

The alumina reduction process is described by the following reaction (Equation (2))

$$2Al_2O_3 + 3C \rightarrow 4Al + 3CO_2 \quad (2)$$

State-of-the-art aluminum production (Hall–Héroult process) consumes about 0.4 kg carbon electrodes, 12.95 kWh of electricity, and 0.4 kg of carbon (from the electrodes) per kg of Al.[33] For the application herein proposed the electric energy consumed, 46.44–46.8 kJ g_{Al}^{-1} according to the current best practice,[42] must originate from RESs.

The high demand for electricity results into indirect CO_2 emissions stemming from power generation, which can vary significantly depending on the viewed country.[43] For example, the global average emissions for primary aluminum production amount to 14.4 $g_{CO2\text{-}eq.}\, g_{Al}^{-1}$ for the entire process chain.[44] From these emissions, about 70% can be attributed to the operation of the Hall–Héroult process. Thus, using electricity based on renewables can significantly reduce the overall emissions. Under these considerations, greenhouse warming potentials (GWP) of renewable-based microgrids may be significantly lower in relation to conventional power and heat production when aluminum is exploited as an energy carrier.[45]

Still, about 1.7 $g_{CO2\text{-}eq.}\, g_{Al}^{-1}$ are generated from the chemical and electrochemical processes occurring in the Hall–Héroult process itself.[44] The literature reports that the substitution of oil-based hard carbon electrodes with biowaste-based hard carbon electrodes, which can be produced by renewable sources, could lead to an almost CO_2 neutral balance.[46] However, this does not eliminate all GWP emissions emitted during the electrolysis. In fact, the carbon-based electrodes react with the molten cryolite-based electrolyte yielding to the emission of perfluorcarbons (PFCs),[47] which are rather strong greenhouse gases. Tetrafluoroethane (CF_4) and hexafluorethane (C_2F_6) correspond to 6630 CO_2 equivalents to 11 100 CO_2 equivalents,[48] respectively (but are also precious fluorochemicals which could be utilized by the chemical industry). The aluminum industry has been able to reduce these PFC emissions from an average of 5 $g_{CO2\text{-}eq.}\, g_{Al}^{-1}$ in 1990 to a value of 0.2 $g_{CO2\text{-}eq.}\, g_{Al}^{-1}$ in 2019 through the use of prebake technology as well as advanced cell management. However, a more definitive solution to lower the greenhouse gas generation in the Hall–Héroult process may only come from the development of inert anodes.[42] Remaining emissions of primary Al production are related to the mining of bauxite (0.03 $g_{CO2\text{-}eq.}\, g_{Al}^{-1}$) and the Bayer process (average of 1.5 $g_{CO2\text{-}eq.}\, g_{Al}^{-1}$).[44] This latter process represents a challenge as it involves the production of red mud as a coproduct (a material consisting of iron, aluminum, and titanium oxides and hydroxides, radionuclides, and heavy metals), which is considered toxic for humans and the environment.[49] However, the use of secondary aluminum and alumina (from the re-electrification) from recycling saves about 92% of the energy related to the Bayer process, strongly reducing the aforementioned CO_2 emissions and the issues related to the red mud.[47]

Recent improvements of Hall–Héroult process have resulted in the aluminum production nowadays to stand rather fluctuating energy supplies. As a matter of fact, aluminum smelting plants are already used for power quality functions as a virtual battery (see, e.g., the TRIMET pilot project in Germany at https://www.greentechmedia.com/articles/read/german-firm-turns-aluminum-smelter-into-huge-battery).

Typically, the molten aluminum produced in the electrolysis cells is periodically siphoned out and placed in holding furnaces to be cast into ingots or shipped in the molten state for specific manufacturing. According to the needs and the availability of RESs, the molten aluminum can be used in several different ways. First, it can act as heat source for heating and cooling networks. Then, it can be cast into ingots for mid- and long-term storage. Also, it can be immediately used for the production of electric energy (according to RES surplus), thus allowing a real integration between the SOFC-based system and the aluminum smelting process.

3. Experimental Section

Aiming to assess the performance of the power systems feed by aluminum powder, a preliminary analysis was conducted using a 0D modeling to compare two different small-scale systems. These were characterized by the integration of either a low-temperature (PEM) or a high-temperature (SOFC) FC technology with an H_2 combustor and steam turbine/GT bottom cycles. The performance of both systems in terms of electrical efficiency and round-trip efficiency (RTE) had been evaluated. The latter, calculated on the basis of the produced power and the specific electric consumption for Al production from alumina, was a critical factor in assessing the economic and environmental utility of the proposed storage technology. A simplified overview of the overall approach is shown in **Figure 1**.

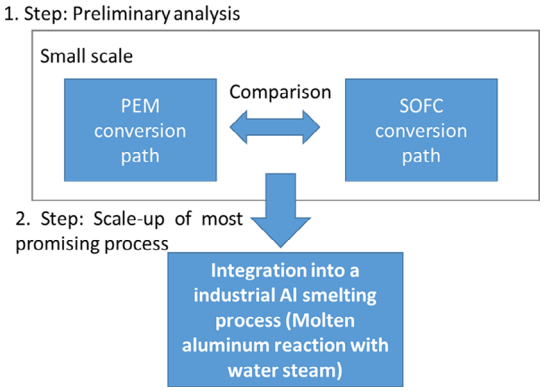

Figure 1. Overview of the applied methodology.

3.1. Preliminary Study

The power plants presented in this section were based on the aluminum combustion reaction reported previously (Equation (1)). As the primary fuel, Al powder with an average particle size of 17.3 μm was considered because it can be oxidized directly in steam.[50] The reaction yields hydrogen and heat, which must be removed from the combustion chamber to maintain a suitable operating temperature. To this aim, a pressurized secondary circuit fed by water was implemented to exploit the combustion heat through superheated steam production and its expansion in a steam turbine. Once separated from alumina, the produced hydrogen can be used to feed a FC, e.g., as discussed in the study by Miller et al.[51] Specifically, both PEM and SOFC technologies had been considered for small-scale applications with installed power in the order of hundreds of kW.

3.1.1. Small-Scale SOFC-Based Plant

The plant layout is shown in **Figure 2**, where the main sections are highlighted. Aluminum and water were the input of the combustion section (A), including the RStoich block "COMBUSTR" to model the aluminum–water reaction of Equation (1). In detail, 33% excess water compared with the stoichiometric value was used to avoid alumina clogging at the inlet of the combustion chamber. The feed water was vaporized and overheated at 350 °C in the heat exchanger "HX1." The produced steam was then used as a carrier for the aluminum powder by premixing these streams before entering the combustion chamber. The reactor outlet temperature (stream "1H") is maintained at 750 °C by a water (stream "3WW")–steam ("4WW") secondary pressurized circuit feeding a steam turbine. The inlet water flow rate "1WW" had been calculated through a design specification procedure to produce overheated steam (stream "4WW") at 450 °C and 12 bar.

The solid aluminum oxide was separated from the hydrogen stream in the block "HX2." The molar composition of the residue stream "1H" consisted of 75 mol% hydrogen and 25 mol% steam.

The FC section (B) was based on the SOFC electrochemical stack model reported by Barelli et al.,[52] implementing the polarization curve relative to the "ASC-800 SOFCPOWER" operating at 850 °C and 2.9 bar (Equation (3)).

$$V = -5.419 \cdot 10^{-08} \cdot I^3 + 2.083 \cdot 10^{-04} \cdot I^2 - 4.596 \cdot 10^{-01} \cdot I + 1.066 \cdot 10^3 \quad (3)$$

where V (mV) and I (mA cm^{-2}) are the operating voltage and current, respectively.

At the SOFC output, the afterburner ("AFTBURN") allowed the total oxidation of the unreacted hydrogen, considering a fuel utilization factor of 0.8. The exhausts from afterburning were expanded in a GT, which activated the compressor to supply pressurized air to the SOFC. The cathode feeding was subsequently preheated by the turbine exhaust ("HX3" heat exchanger) and then heated up to 800 °C through the cathodic thermal regeneration ("REG" heat exchanger).

The GT (section (C)) consisted of a CAPSTONE C30[53,54] GT, which was a single shaft micro-GT equipped with a centrifugal compressor and a radial turbine. The GT datasheet parameters are shown in **Table 2**. To evaluate the power output of the GT under different operating conditions, Equation (3)–(7) were used. It is worth highlighting that the achievable turbine power output was higher than the nominal (30 kW) reported in the datasheet, due to the higher specific heat of the inlet stream ("1G")

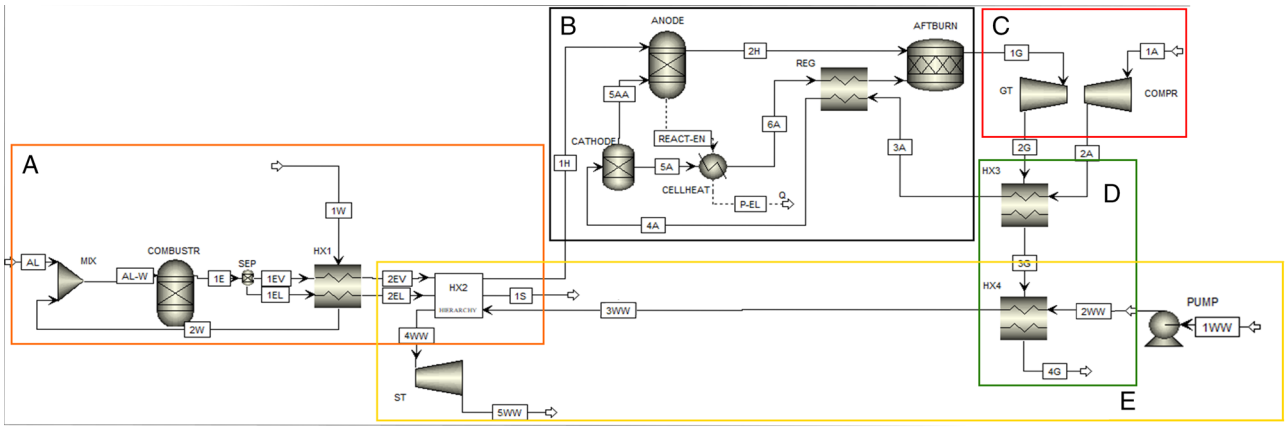

Figure 2. SOFC plant layout: A) combustor section, B) SOFC section, C) GT, D) heat recovery, E) steam turbine.

Table 2. Capstone C30 nominal data referred to methane combustion.

Pressure ratio	3.2
Compressor isentropic efficiency	80%
Air flow rate	0.31 kg s^{-1}
Fuel flow rate	0.0024 kg s^{-1}
Turbine inlet temperature	900 °C
Turbine isentropic efficiency	90%
Electric power generated	30 kW
Electric efficiency	26%

compared with the exhaust gases obtained through methane combustion under the operating condition of Table 2.

$$\text{Compressor pressure ratio}: \beta_c = \frac{p_{2A}}{p_{1A}} \tag{4}$$

$$\text{Compressor power}: W_c = \dot{m}_{1A} \cdot C_{p,1A} \cdot T_{1A} \cdot \left(\beta_c^{\frac{k_{1A}-1}{k_{1A}}} - 1\right) \tag{5}$$

$$\text{Turbine pressure ratio}: \beta_t = \frac{p_{2G}}{p_{1G}} \tag{6}$$

$$\text{Turbine power}: W_t = \dot{m}_{1G} \cdot C_{p,1G} \cdot T_{1G} \cdot \left(1 - \beta_t^{\frac{k_{1G}-1}{k_{1G}}}\right) \tag{7}$$

The power of the GT had been calculated through Equation (8)

$$W_{GT} = \eta_t \cdot W_t - \frac{W_c}{\eta_c} \tag{8}$$

where the compressor (η_c) and turbine isentropic efficiency (η_t) have been set to 0.8 and 0.9, respectively.

The heat-recovery section had been designed to exploit the turbine exhaust, increasing the overall efficiency of the system. To this aim, two heat exchangers had been used for preheating the FC feeding air ("HX3") and the water in the pressurized secondary circuit ("HX4"), respectively.

3.1.2. Small-Scale PEM-Based Plant

The PEM-based plant system is shown in **Figure 3**. The layout of the aluminum combustor section (A) was rather similar to that of the SOFC plant. The only difference resided in the combustor outlet operating temperature (stream "1H") being 400 °C, i.e., lower than in the SOFC layout (750 °C). Theoretically, a lower temperature could be used considering the low PEM operative temperature. However, temperatures lower than 400 °C would favor the unwanted formation of boehmite, compromising the neutrality of the proposed P2P application. In fact, bauxite rather than boehmite was needed for the upstream metallurgical alumina production via the Hall–Héroult process. Downstream of the heat exchangers ("HX1" and "HX2") used for the aluminum combustor cooling, solid "1S" and gaseous "1H" (steam and hydrogen mixture) products were separated.

To condense the water present in the hot hydrogen–water stream ("1H"), this was first cooled down in "HX3" and "HX4" heat exchangers and, then, flushed at ambient temperature ("FLASH" block). Moreover, "HX3" and "HX4" allowed, respectively, to heat-up the FC feeding hydrogen to 70 °C (stream "4 H") and to preheat the water ("2WW") in the pressurized secondary circuit.

In this model, the PEM FC (section (B)) was operated at 70 °C and ambient pressure making the implementation of the GT inconvenient. For this reason, the anodic off-gases recirculation had been implemented to adjust the system fuel utilization factor at 0.85 at a parity of the stack fuel utilization factor (0.8).

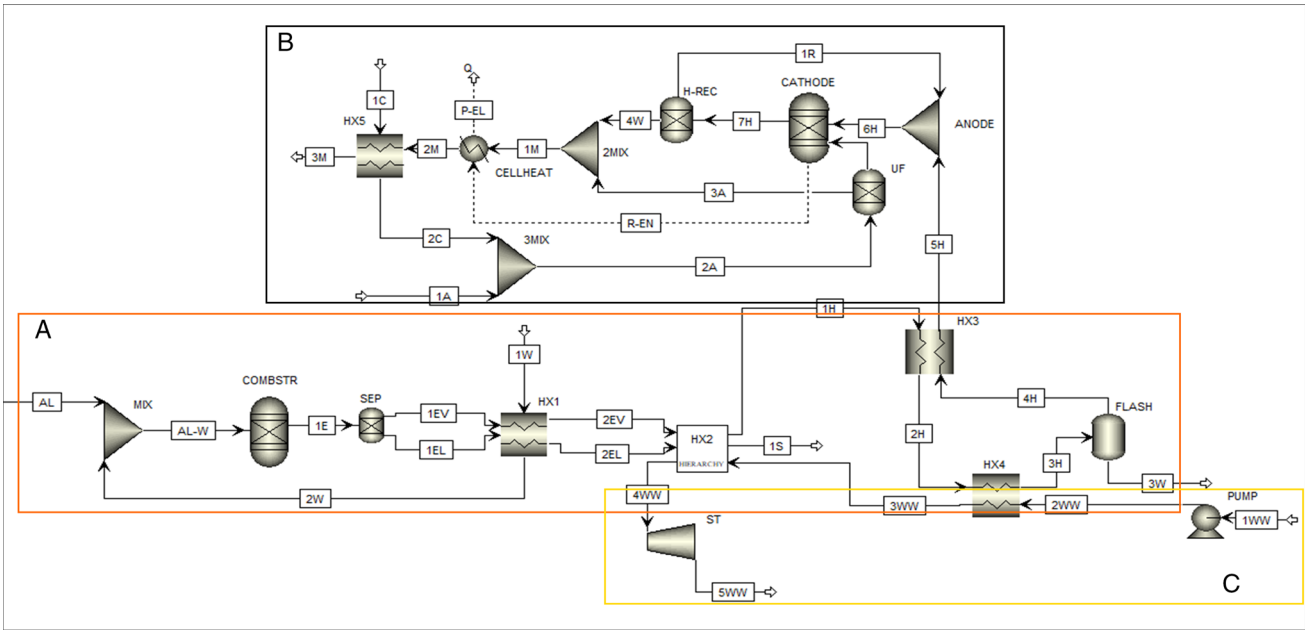

Figure 3. PEM plant layout: A) combustor section, B) PEM FC section, C) secondary heat recovery section.

Consequently, the anodic feeding stream ("6H") consisted of the hydrogen from the aluminum combustion ("5H") and the unreacted hydrogen in the recirculated anode off-gases ("1R").

The PEM FC worked with a relative humidification (RH) of the inlet air to 100% to avoid membrane degradation and, at the same time, to assure optimal operating conditions. In particular, the equations that estimated the PEM operative voltage and current were shown in the study by Barelli et al.[55] The FC was cooled by the water stream "1C" (heat exchanger "HX5") that it successively mixed with the FC feeding air ("1A"). The flow rate of "1C" was regulated to match the set RH in the stream "2A."[55]

The produced electric power ("P-EL") had been set in a Fortran subroutine[55] that regulated the input aluminum flow rate to match the desired value. Finally, the "CELLHEAT" block had been used to simulate the thermal power generated by the exothermic reactions occurring in the stack.

The secondary water circuit section (area "C" of Figure 3) had the following functions: 1) heat recovery for power production in a steam turbine ("ST"); 2) cooling the exhausted aluminum combustor ("HX4"); and 3) control the temperature in the combustion chamber ("HX2" heat exchanger). As for the SOFC-based plant mentioned earlier, the water (stream "1WW") flow rate had been calculated to produce overheated steam at 450 °C and 12 bar.

3.2. Results of the Preliminary Study

To analyze the overall performance of the two power plants described in Section 3.1, the operating conditions of each plant section are presented in the following. All details are reported in the Supporting Information. Specifically, the input/output streams of the aluminum combustor section are shown in Table S1 and S2, Supporting Information, for the SOFC- and PEM-based plants, respectively. The detailed results relative to the FC sections are reassumed in Table S3, Supporting Information (SOFC) and Table S4, Supporting Information (PEM FC). For completeness, Table S5, Supporting Information, reports the results obtained for the gas and steam turbine bottom sections for the SOFC system, where a produced power of 38.3 and 30.8 kW was calculated, respectively. Finally, Table S6, Supporting Information, shows the inlet/outlet streams of the 37.6 kW steam turbine implemented in the PEM system.

The global results obtained from the simulation of both the SOFC- and PEM-based plants are shown in **Table 3**. Specifically, the produced power values in each section together with the plant electrical efficiency $\eta_{(I)}$ (Equation (9)) and RTE (Equation (10)) are indicated.

$$\eta_{(I)} = \frac{P_{tot}}{P_{input}} = \frac{P_{FC} + P_{GT} + P_{ST}}{\dot{m}_{AL} \cdot LHV_{AL}} \quad (9)$$

Table 3. Global results of SOFC- and PEM-based power plants.

Power plant	$\dot{m}_{AL}$ [g s^{-1}]	P_{input} [kW]	$P_{smelting}$ [kW]	P_{FC} [kW]	P_{GT} [kW]	P_{ST} [kW]	P_{tot} [kW]	$\eta_{(I)}$ [%]	RTE [%]
AL-SOFC	12.5	223.5	607.5	90	38.3	30.8	159.1	71.2	26.2
AL-PEM	12.5	223.5	607.5	95	–	37.6	132.6	59.3	21.8

$$RTE = \frac{P_{tot}}{P_{smelting}} = \frac{P_{FC} + P_{GT} + P_{ST}}{\dot{m}_{AL} \cdot E_{smelting}} \quad (10)$$

where P_{tot} stands for the expected produced power plant (kW) calculated as the sum of the FC (P_{FC}), GT (P_{GT}), and steam turbine (P_{ST}) generated power values. P_{input} represents the input power evaluated in terms of the aluminum low heating value (LHV_{Al} of 17 874 kJ kg^{-1}), whereas $P_{smelting}$ is the power corresponding to the primary aluminum smelting energy intensity, i.e., the electric specific consumption of the Hall–Héroult process ($E_{smelting}$) set at 48.6 kJ g_{Al}^{-1} as resulting from the most recent statistical data (year 2019) available for China.[56] This country was chosen since, according to the available data relative to the period June 2018–May 2019, it accounted for about 57% of the worldwide primary aluminum production.[57]

The SOFC-based plant was characterized by 20% more power than the PEM-plant fed with the same Al flow rate due to the GT implementation. As expected, a positive impact on both $\eta_{(I)}$ and RTE is observed: the SOFC plant achieves an efficiency greater than 70% and an RTE of about 26% compared with about 59% and 21.8% for the PEM-based plant. However, it should be noted that due to anodic recirculation, the PEM FC exploited hydrogen more efficiently with an electrical power output of 95 kW (versus 90 kW of the SOFC). Anyway, the higher operating temperature and pressure of the SOFC made convenient the implementation of a bottom GT, allowing a higher total produced power with consequent greater $\eta_{(I)}$ and RTE values.

3.3. Scale-Up of the Plant

As detailed in Section 3.2, the aluminum powder exploitation in the SOFC-based plant resulted more promising regarding to $\eta_{(I)}$ and RTE. Thus, the evaluation of the SOFC-based aluminum conversion technology was further developed to a larger scale. In addition, the conversion of the Al carrier for power production was assessed in a direct integration with the smelting plant (based on the Hall–Héroult process) to make use of the molten aluminum storage available.

The plant sizing had been designed based on the average annual aluminum production of the German smelting plants estimated in about 130 000 tons.[41] The SOFC of 2 MW installed power with a feeding flow rate of 275.9 g s^{-1} had been selected, which corresponded to 6.4% of the average annual production for each factory.

To this aim, the system layout already described in the previous section was optimized to use molten aluminum as the feeding carrier and to integrate GT and ST technologies available for power sizes in the MW order. Using molten aluminum offers the great advantage to avoid the safety risk associated with fine aluminum powder production (e.g., explosion[58]).

Accordingly, the SOFC model had been updated and slightly modified considering the molten aluminum feed at 900 °C. In terms of plant layout, the only difference compared with the SOFC system of Figure 2 was the presence of an additional heat recovery section between the molten aluminum and the water stream in the secondary pressurized circuit. This thermal recovery allowed the system to bring the steam turbine inlet

Table 4. Global results of scaled-up SOFC-based power plan.

Power plant	$\dot{m}_{AL}$ [g s^{-1}]	$P_{smelting}$ [kW]	P_{FC} [kW]	P_{GT} [kW]	P_{ST} [kW]	P_{tot} [kW]	RTE [%]
Molten AL-SOFC	275.91	13 408	2000	906.4	1064	3970	29.6

temperature at 550 °C by tansimuleously maintaining aluminum in the molten state at the combustor inlet (750 °C).

4. Results and Discussion

The upscaled SOFC plant performance is shown in **Table 4**. The use of molten aluminum enables higher energy efficiency values than those obtained for the small-scale SOFC plant. In more detail, implementing a 2 MW FC results in an overall power generation of 4 MW through the contribution of the GT (906 kW) and the ST (1064 kW) sections. Considering the electric power for the smelting process of the Al flow as input (13.4 MW), the RTE resulting from the use of molten aluminum increases from 26.2% (Table 3) to 29.6% (Table 4).

We highlight that this assessment is based on the current primary aluminum smelting energy data from China in 2017, even though the current best practice of Hall–Héroult electrolysis cells use only 46.44–46.8 kJ g_{Al}^{-1} (i.e., about 4% less).[42] Moreover, a significant progress of energy efficiency is expected in the near future, according to the prospective scenarios for the aluminum industry defined by the European Commission, in particular for energy and greenhouse gas emissions.[42] Several innovative technologies are foreseen regarding aluminum smelting. Among these, cathodes made from materials (e.g., TiB_2) wet by molten aluminum to allow for optimal drainage (also called wettable drained cathodes). The use of such wettable drained cathode technology would allow the reduction of the anode–cathode distance, which represents one of the main causes of inefficiency by Ohmic drop; the potential energy savings are estimated at 15–20% with respect to the current best practice.[42] Improvements can be further achieved through the implementation of inert and dimensionally stable noncarbon anodes because they are not consumed in the electrolytic process. The combined implementation of these technologies in the Hall–Héroult process is expected to reduce energy requirements in the electrolysis and anode manufacturing processes by 11 kJ g_{Al}^{-1}. These improvements would further favor the exploitation of aluminum as energy storage medium and carrier through the P2P application proposed here. Assuming a precautionary reduction of the specific consumption by 15% with respect to the state of the art smelters, the RTE for the utilization of Al in P2P applications could rise to about 36.3% with a volumetric energy density storage of 23.5 kWh L^{-1}.

In the following, the proposed technology is compared with alternative P2P applications based on the exploitation of hydrogen or liquid fuels as ESCM suitable for medium- and long-term storage. Regarding hydrogen, RTEs of about 30% can be achieved with systems including PEM electrolyzers and PEM stacks, but with a hydrogen storage pressure of 200 bar, i.e., corresponding to a specific energy of only 0.53 kWh L^{-1} at ambient temperature.[6] Advanced systems based on the reversible solid oxide technology result in higher RTEs (48%),[51] but they are assessed under a hydrogen storage pressure of 70 bar, i.e., offering an even lower volumetric energy density, i.e., around 0.2 kWh L^{-1} at ambient temperature. It is also remarked that the performance of the reversible solid oxide stacks is affected by degradation phenomena when operating for both power storage (electrolyzer) and power generation (FC), which have not been thoroughly investigated.

Regarding P2P applications characterized by higher volumetric energy and easier management of the ESCM, chemical storage based on liquid fuels produced from RES should be considered for further comparative assessments. However, switching from H_2 to liquid fuel ESCMs leads to a decrease in RTE because the conversion of hydrogen into a liquid fuel (e.g., methanol, dimethyl ether (DME), and gasoline) will introduce an additional efficiency factor of about 0.7–0.8.[59] In case methanol/DME and gasoline are considered as carriers, the efficiency of the power-to-fuel process via solid oxide electrolyzers (SOE) decreases to 66% and 60%, respectively, based on the low heating value.[59] Moreover, efficiency reductions are also expected for the re-electrification of the liquid fuels even using highly efficient electrochemical converters (e.g., SOFC). For optimized SOFC-based plants, a fuel-to-power efficiency of up to 55% maybe achieved with direct methanol feeding, i.e., with a decrease of about 5%[60] compared with the natural gas feeding.[61] Instead, an efficiency of only 45% can be assumed for small-scale systems related to gasoline-fueled SOFC.[62] Correspondingly, RTE values are 36% and 27% for methanol/DME and gasoline, respectively.

Finally, due to the existing infrastructure, the conversion of renewable energy to liquefied natural gas (LNG) is considered very interesting. Power-to-LNG via electrolysis, methanation, methane separation, and liquefaction processes may achieve energy efficiencies as high as 46.3%,[63] whereas the power production through SOFC-based plants exhibits 60%,[64] resulting in ≈28% RTE.

Table 5 and **Figure 4** compare the RTE and volumetric energy density values of the considered ESCM, highlighting

Table 5. RTE, volumetric energy density, and implemented technologies of P2P applications based on different energy carriers. The RTE values in brackets include the thermal (1750 kWh/t_{CO2}) and electric (250 kWh/t_{CO2}) specific consumptions for CO_2 direct air capture for low-temperature solid sorbent technologies.[65]

Energy carrier	Conversion technology	RTE	Vol. energy [kWh L^{-1}]
Al	System proposed in Section 3.2	36.3%	23.5
H_2	PEM electrolyzer/PEM fuel cell	30%	0.53
	rSOC	48%	0.2
Methanol/DME	SOE/SOFC	36% (26.5%)	5.5
Gasoline	SOE/SOFC	27% (20%)	8.8
LNG	SOE/TSA dehydration, H_2 and CO_2 membrane separation/SOFC	28% (23%)	5.8

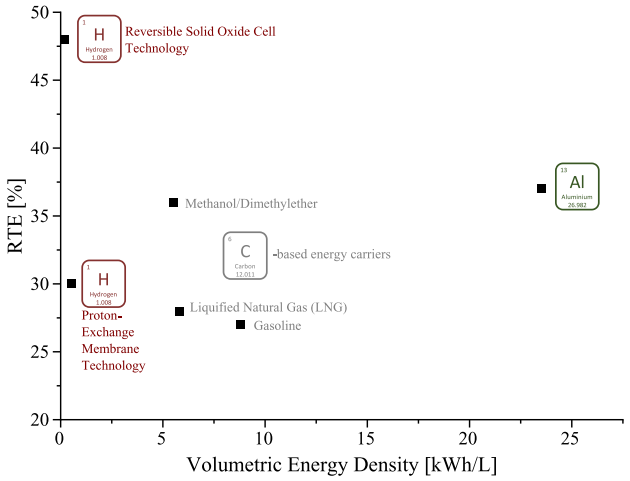

Figure 4. RTE and volumetric energy density of alternative P2P applications based on chemical storage by exploiting different ESCMs.

the relevance of aluminum, especially in terms of volumetric energy density.

5. Conclusion

The shift from fossil fuels to RES requires appropriate system flexibility to bridge the geographical and temporal availability and variability of RES. One of the key issues to achieve such a flexibility is the realization of sector coupling in multienergy systems to integrate multiple energy vectors and sectors. Therefore, the identification of new ESCMs, enabling energy storage and intersectoral applications at the users' side, plays a key role. Green hydrogen, i.e., produced only from RES, is considered as one of the most promising ESCM, but its rather low volumetric energy density and safety issues have driven the research toward the analysis of new energy carriers.

In this context, the use of aluminum as ESCM has been explored herein, including the development of high-efficiency power plants for its re-electrification. In a preliminary analysis, two small-scale power systems have been analyzed which are characterized by the integration of an aluminum combustor, a PEM or SOFC FC, a hydrogen combustor with gas and steam turbine bottom cycles. Two 0-D models have been implemented to estimate their performance. The results clearly indicate higher $\eta_{(I)}$ and RTE values for the SOFC-based plant (71% and 26.2%, respectively) with respect to the PEM-based system, (59% and 22%, respectively).

On this basis, the evaluation has been scaled-up to a MW system including molten aluminum feeding, which is of interest for the system integration in refining aluminum factories. In this way, even higher energy performance compared with the small-scale SOFC plant were obtained. Specifically, implementing a 2 MW FC, which needs 275.9 g s^{-1} Al flow as input, almost 4 MW of electric power is produced considering the additional power delivered by the bottom cycles (906.4 kW by the GT, 1064 kW by the ST). This performance improvement corresponds to a further increase in RTE (P2P) to about 30% based on the actual energy consumption available from the aluminum industry. In addition, such an interesting performance could rise even further (36.3%) according to the expected technological developments in the aluminum production. Obviously, these RTEs have to be proven on a demonstration level to verify preliminary modeling results.

Nonetheless, the proposed approach based on aluminum appears to compete with P2P systems based on hydrogen implementing low and high temperature electrolyzers, especially in terms of storage needs (23.5 kWh L^{-1} volumetric energy density) and safety (aluminum, e.g., as ingots, is neither toxic nor dangerous when stored). Moreover, the achieved RTE and volumetric energy density offered by aluminum appears to be competitive with liquid fuels. From the social acceptance point of view, aluminum is expected to outperform both hydrogen and liquid fuels, being safe, nontoxic, nonflammable and already widely present in our daily life.

Overall, the use of aluminum as energy carrier for chemical storage can significantly contribute to a further increase in RES shares while reducing the EU dependence on imported fuels. In addition, the industry related to metal production in Europe (most of the reactive metals are available in the EU countries) can be strengthened while enhancing sustainability. The power generation sector will benefit as novel combinations of gas/steam turbines, FCs, and primary batteries have the potential to be developed as well. In general, the development of inert anodes and the use of renewable generated energy for the Hall–Héroult process is a precondition for this development.

To better assess the feasibility of the proposed new paradigm, further studies beyond the energy efficiency need to be performed to exploit all optimization steps for the aluminum production (e.g., used electrodes, and cryolite). This should include a first life cycle assessment and technoeconomic analysis to unveil the potential environmental and economic benefits (or hotspots) of the presented solution in comparison with other P2P paths in view of circular economy (e.g., impacts of reducing the energy demand for primary aluminum). Extremely important is also the exploitation of aluminum as energy storage and carrier medium directly in primary batteries, which would result in even higher energy efficiencies. In addition, the stored metal could be integrated in district heating and cooling, using, e.g., water–ammonia heat pumps. Finally, other abundant reactive metals such as magnesium, zinc, and even sodium could be exploited as energy storage media and carriers as alternative to hydrogen and other liquid or gaseous fuels.

Supporting Information

Supporting Information is available from the Wiley Online Library or from the author.

Acknowledgements

Open-access funding enabled and organized by Projekt DEAL.

Conflict of Interest

The authors declare no conflict of interest.

Author Contributions

L.B. and A.O. conceived and designed the simulations; moreover, they wrote the manuscript. L.B. analyzed the obtained data after simulation implementation with respect to alternative P2P technologies based on chemical storage. A.O. and L.T. implemented and performed the simulations and contributed to the description of the state of the art. G.B. and R.S. reviewed the manuscript. M.B. analyzed the broader context for the exploitation of reactive metals as energy carriers and reviewed the manuscript. S.P. conceived the possible scenarios and strategies for reactive metals implementation in the mid- and long-term energy storage in view of cross-sectoral systems and multiple users feeding and reviewed the manuscript.

Keywords

aluminum energy carriers, aluminum steam combustion, electric energy storage, reactive metals, solid oxide fuel cells

Received: March 12, 2020
Revised: May 14, 2020
Published online:

[1] U. S. Energy Information Administration, *Annual Energy Outlook 2019 with Projections to 2050*, U. S. Energy Information Administration, Washinton, DC **2019**, pp. 1–64.
[2] M. Olczak, A. Piebalgs, *Sector Coupling: The New EU Climate and Energy Paradigm? FSR Energy – Florence School Regulation*, EUI, Florence **2018**.
[3] M. Mazengarb, Hydrogen re-fuelling station explodes in Norway, Hyundai and Toyota suspend fuel cell sales, https://reneweconomy.com.au/hydrogen-re-fuelling-station-explodes-in-norway-hyundai-and-toyota-suspend-fuel-cell-sales-99377/ (accessed: July 2019).
[4] G. Zhao, A. S. Pedersen, *Proc. CIRP* **2018**, *69*, 529.
[5] J. M. Bergthorson, Y. Yavor, J. Palecka, W. Georges, M. Soo, J. Vickery, S. Goroshin, D. L. Frost, A. J. Higgins, *Appl. Energy* **2017**, *186*, 13.
[6] M. A. Pellow, C. J. M. Emmott, C. J. Barnhart, S. M. Benson, *Energy Environ. Sci.* **2015**, *8*, 1938.
[7] M. Gurz, E. Baltacioglu, Y. Hames, K. Kaya, *Int. J. Hydrogen Energy* **2017**, *42*, 23334.
[8] IEA, The future of hydrogen. https://webstore.iea.org/the-future-of-hydrogen (accessed: July 2019).
[9] L. Barelli, G. Bidini, A. Ottaviano, *Energy* **2015**, *90*, 1180.
[10] Cause found for fire at H2 refilling station in Norway, **2019**, https://www.electrive.com/2019/07/01/cause-found-explosion-at-h2-refuelling-station-in-norway/ (accessed: April 2020).
[11] F. Barbir, in *PEM Fuel Cells*, Elsevier, London **2013**, pp. 373–434.
[12] A. Baroutaji, T. Wilberforce, M. Ramadan, A. G. Olabi, *Renewable Sustainable Energy Rev.* **2019**, *106*, 31.
[13] A. Sartbaeva, V. L. Kuznetsov, S. A. Wells, P. P. Edwards, *Energy Environ. Sci.* **2008**, *1*, 79.
[14] S. S. Makridis, in *Methane and Hydrogen for Energy Storage*, The Institution of Engineering and Technology, London **2016**.
[15] M. Gambini, T. Stilo, M. Vellini, *Int. J. Hydrogen Energy* **2019**, *44*, 15118.
[16] H.-W. Li, M. Zhu, C. Buckley, T. Jensen, *Inorganics* **2018**, *6*, 91.
[17] H. Wang, X. Zhou, M. Ouyang, *Int. J. Hydrogen Energy* **2016**, *41*, 18062.
[18] Y. Shen, Y. Zhan, S. Li, F. Ning, Y. Du, Y. Huang, T. He, X. Zhou, *Chem. Sci.* **2017**, *8*, 7498.
[19] D. J. Durbin, C. Malardier-Jugroot, *Int. J. Hydrogen Energy* **2013**, *38*, 14595.
[20] M. Behrens, *Recycl. Catal.* **2016**, *2*, 78.
[21] S. A. Mohamed, F. A. Al-Sulaiman, N. I. Ibrahim, M. H. Zahir, A. Al-Ahmed, R. Saidur, B. S. Yılbaş, A. Z. Sahin, *Renewable Sustainable Energy Rev.* **2017**, *70*, 1072.
[22] A. Valera-Medina, H. Xiao, M. Owen-Jones, W. I. F. David, P. J. Bowen, *Prog. Energy Combust. Sci.* **2018**, *69*, 63.
[23] J. Yang, A. F. S. Molouk, T. Okanishi, H. Muroyama, T. Matsui, K. Eguchi, *ACS Appl. Mater. Interfaces* **2015**, *7*, 28701.
[24] K. E. Lamb, M. D. Dolan, D. F. Kennedy, *Int. J. Hydrogen Energy* **2019**, *44*, 3580.
[25] B. Stoeckl, V. Subotić, M. Preininger, M. Schwaiger, N. Evic, H. Schroettner, C. Hochenauer, *Electrochim. Acta* **2018**, *298*, 874.
[26] A. M. Kler, E. A. Tyurina, Y. M. Potanina, A. S. Mednikov, *Int. J. Hydrogen Energy* **2015**, *40*, 14775.
[27] E. I. Shkolnikov, A. Z. Zhuk, M. S. Vlaskin, *Renewable Sustainable Energy Rev.* **2011**, *15*, 4611.
[28] Y. Yavor, S. Goroshin, J. M. Bergthorson, D. L. Frost, R. Stowe, S. Ringuette, *Int. J. Hydrogen Energy* **2013**, *38*, 14992.
[29] Y. Yavor, S. Goroshin, J. M. Bergthorson, D. L. Frost, *Int. J. Hydrogen Energy* **2015**, *40*, 1026.
[30] A. V. Bersh, A. V. Lisitsyn, A. I. Sorokovikov, M. S. Vlaskin, Y. A. Mazalov, E. I. Shkol'nikov, *High Temp.* **2010**, *48*, 866.
[31] L. Soler, J. Macanás, M. Muñoz, J. Casado, *J. Power Sources* **2007**, *169*, 144.
[32] T. Hiraki, S. Yamauchi, M. Iida, H. Uesugi, T. Akiyama, *Environ. Sci. Technol.* **2007**, *41*, 4454.
[33] G. N. Ambaryan, M. S. Vlaskin, A. O. Dudoladov, E. A. Meshkov, A. Z. Zhuk, E. I. Shkolnikov, *Int. J. Hydrogen Energy* **2016**, *41*, 17216.
[34] V. Rosenband, A. Gany, *Int. J. Hydrogen Energy* **2010**, *35*, 10898.
[35] S. Elitzur, V. Rosenband, A. Gany, *Int. J. Hydrogen Energy* **2014**, *39*, 6328.
[36] O. V. Kravchenko, K. N. Semenenko, B. M. Bulychev, K. B. Kalmykov, *J. Alloys Compd.* **2005**, *397*, 58.
[37] J. T. Ziebarth, J. M. Woodall, R. A. Kramer, G. Choi, *Int. J. Hydrogen Energy* **2011**, *36*, 5271.
[38] M. S. Vlaskin, E. I. Shkolnikov, A. V. Bersh, *Int. J. Hydrogen Energy* **2011**, *36*, 6484.
[39] M. S. Vlaskin, A. O. Dudoladov, O. A. Buryakovskaya, G. N. Ambaryan, *Int. J. Hydrogen Energy* **2018**, *43*, 4623.
[40] M. S. Vlaskin, A. Z. Zhuk, V. I. Miroshnichenko, A. E. Sheindlin, *High Temp.* **2018**, *56*, 774.
[41] G. E. Totten, D. S. MacKenzie, *Handbook of Aluminum: Vol. 2: Alloy Production and Materials Manufacturing*, Choice Rev. Online, CRC Press, Boca Raton **2013**.
[42] Energy efficiency and GHG emissions: prospective scenarios for the aluminium industry, https://setis.ec.europa.eu/sites/default/files/reports/energy_efficiency_and_ghg_emissions.pdf (accessed: July 2019).
[43] D. Paraskevas, K. Kellens, A. Van De Voorde, W. Dewulf, J. R. Duflou, *Proc. CIRP* **2016**, *40*, 209.
[44] G. Saevarsdottir, H. Kvande, B. J. Welch, *JOM* **2020**, *72*, 296.
[45] M. Haller, D. Carbonell, M. Dudita, D. Zenhäusern, A. Häberle, *Energy Convers. Manag. X* **2019**, *5*, 100017.
[46] A. Baldinelli, X. Dou, D. Buchholz, M. Marinaro, S. Passerini, L. Barelli, *Green Chem.* **2018**, *20*, 1527.
[47] M. Jinlong Wang, The Environmental Footprint of Semi-Finished Aluminum Products in North America: A Life Cycle Assessment Report, **2013**. https://www.aluminum.org/sites/default/files/LCA_Report_Aluminum_Association_12_13.pdf (accessed: June 2020).

[48] T. F. Stocker, D. Qin, G. K. Plattner, M. M. B. Tignor, S. K. Allen, J. Boschung, A. Nauels, Y. Xia, V. Bex, P. M. Midgley, *Climate Change 2013: The Physical Science Basis: Working Group I Contribution to the Fifth Assessment Report of the Intergovernmental Panel on Climate Change*, Cambridge University Press, Cambridge **2013**.
[49] M. Mišík, I. T. Burke, M. Reismüller, C. Pichler, B. Rainer, K. Mišíková, W. M. Mayes, S. Knasmueller, *Sci. Total Environ.* **2014**, *493*, 883.
[50] J. Foote, B. Thompson, J. Lineberry, in *Advances in Chemical Propulsion: Science to Technology*, CRC Press, Boca Raton **2010**.
[51] T. F. Miller, J. L. Walter, D. H. Kiely, in *Proc. 2002 Workshop on Autonomous Underwater Vehicles*, IEEE, Piscataway, NJ **2002**, pp. 111–119.
[52] L. Barelli, G. Bidini, A. Ottaviano, *Int. J. Hydrogen Energy* **2012**, *37*, 16140.
[53] L. Barelli, G. Bidini, A. Ottaviano, *Appl. Energy* **2013**, *110*, 173.
[54] L. Barelli, G. Bidini, A. Ottaviano, *Energy* **2017**, *118*, 716.
[55] L. Barelli, G. Bidini, F. Gallorini, A. Ottaviano, *Int. J. Hydrogen Energy* **2011**, *36*, 10434.
[56] The International Aluminium Institute, Primary Aluminium Smelting Energy Intensity, http://www.world-aluminium.org/statistics/primary-aluminium-smelting-energy-intensity/ (accessed: June 2020).
[57] The International Aluminium Institute, Primary Aluminium Production, http://www.world-aluminium.org/statistics/primary-aluminium-production/ (accessed: June 2020).
[58] H. Chen, Y. Zhang, H. Liu, X. Meng, W. Du, *J. Loss Prev. Process Ind.* **2018**, *55*, 19.
[59] L. Wang, M. Chen, R. Küngas, T. E. Lin, S. Diethelm, F. Maréchal, J. Van Herle, *Renew. Sustainable Energy Rev.* **2019**, *110*, 174.
[60] M. Rokni, L. R. Clausen, C. Bang-Møller, in *52th Int. Conf. of Scandinavian Simulation Society*, Mälardalen University, Västerås **2011**.
[61] Solid Power, BlueGen the world's most efficient micro-CHP. https://www.solidpower.com/fileadmin/user_upload/pages/Logos_materialien/SOLIDpower_BlueGEN_Brochure_UK_web.pdf (accessed: August 2019).
[62] H. Dhingra, B. A. Peppley, *J. Power Sources* **2013**, *239*, 527.
[63] E. A. Morosanu, A. Saldivia, M. Antonini, S. Bensaid, *Energy Fuels* **2018**, *32*, 8868.
[64] Solid Power, BlueGen: The World's Most Efficient Micro-CHP https://www.solidpower.com/fileadmin/user_upload/pages/Logos_materialien/SOLIDpower_BlueGEN_Brochure_UK_web.pdf (accessed: June 2020).
[65] M. Fasihi, O. Efimova, C. Breyer, *J. Cleaner Prod.* **2019**, *224*, 957.

